IF 51 (291)
"PLY STEER"

IN SITU MEASUREMENT OF TIRE PLY STEER BASED ON AN INTELLIGENT TIRE SYSTEM

YAN WANG,[1] ZHE LIU,[1] HAO WANG,[2] MICHAEL KALISKE,[3] YINTAO WEI[1,*]

[1]SCHOOL OF VEHICLE AND MOBILITY, TSINGHUA UNIVERSITY, BEIJING, CHINA
[2]E-RUBBER TECHNOLOGY (BEIJING) CO., LTD., BEIJING, CHINA
[3]INSTITUTE FOR STRUCTURAL ANALYSIS, TECHNISCHE UNIVERSITÄT DRESDEN, DRESDEN, GERMANY

RUBBER CHEMISTRY AND TECHNOLOGY, Vol. 94, No. 1, pp. 180–199 (2021)

ABSTRACT

Ply steer is an inherent property of a belted tire, manifesting as the nonzero side force at a slip angle of zero, and it is thus an important design factor relevant to a vehicle's straight running, safety, and comfort. Although ply steer is a rolling contact phenomenon, there is a lack of approaches for direct measurement and modeling of tire ply steer force in motion. Thus, we developed an in situ measurement method for tire ply steer based on a recently proposed accelerometer-based intelligent tire system. This new measurement method is significant for three main reasons: it facilitates understanding of the inherent mechanism of ply steer for radial tires, it improves the intelligent tire's accuracy based on the accelerometer, and it provides an in situ measurement approach for tire ply steer. An accelerometer-based intelligent tire was developed to obtain acceleration measurements at different conditions in which the lateral behavior is of particular interest. Two unusual phenomena that have never been reported are observed: (1) lateral accelerations demonstrate asymmetrical behavior with respect to positive/negative slip angles and (2) lateral accelerations at zero slip angle still exist. It is hypothesized that the underlying reason for these two unusual phenomena is the ply steer–dependent kinematics, which can conversely be used to measure tire ply steer in situ. To this end, the mixed Lagrange–Euler approach for rolling contact kinematics is used to formulate tire lateral acceleration, which links both rigid motion and elastic displacement. It is clearly found that the lateral acceleration is proportional to the square of the rotating velocity and the second-order gradient of displacement. Based on this kinematic model, the features of lateral acceleration can be easily explained by tire ply steer, which manifests as the sinusoidal lateral deformation modes due to the coupling of the bending-twist deformation of the cord–rubber composites of the tire belt. The proposed hypothesis has been verified by finite element method simulations, and the experimental results prove that tire ply steer leads to the observed unusual lateral acceleration pattern. Thus, the quantitative value of ply steer could be measured in situ by integrating the obtained lateral acceleration and thus the apparent elastic slip angle, even under zero external wheel slip angle. In this manner, the intelligent tire system provides a direct measurement approach for tire ply in motion. In addition, the accuracy of the intelligent tire's algorithm might be improved by suitable modeling of the asymmetrical acceleration with respect to left/right slip based on the proposed hypothesis of ply steer–dependent kinematics.
[doi:10.5254/RCT.20.80381]

INTRODUCTION

With the increasing investment in autonomous vehicles and connected vehicles, intelligent tires have received increasing attention worldwide[1] and can be used to sense tire forces and moment,[2] slip angle,[3] tire–road friction coefficient,[4–6] hydroplaning,[7] noise and vibration,[8] fatigue, cracking,[9] and so forth.

Different types of sensors have been used to develop intelligent tire systems, including optical sensors,[10,11] laser sensors,[12] capacitance sensors,[13–16] strain gauges,[17–19] magnetic sensors,[20] and accelerometers,[21,22] among which the micro-electro-mechanical system (MEMS) accelerometer has attracted special interest because of its lightweight, robust, and cost-effective design. Several researchers, including Brusarosco,[21,22] Erdogan,[23] Tuononen,[24] and Singh,[4,6] have developed accelerometer-based intelligent tires to estimate tire forces, tire–road coefficients, and other important parameters. Therefore, the accelerometer is chosen to establish the intelligent tire system.

In addition to the mentioned application of the intelligent tire, this study has found a special and novel application: in situ measurement of tire ply steer. Ply steer is an inherent property of a belted

*Corresponding author. Email: weiyt@tsinghua.edu.cn

สำเนาเพื่อใช้ในการศึกษาเท่านั้น

Downloaded from http://meridian.allenpress.com/rct/article-pdf/94/1/180/2807318/0035-9475-94-1-180.pdf by Ministry of Science and Technology (Thailand) user on 25 May 2022

FIG. 1. — Intelligent tire system and data transmitted wirelessly.

tire, manifesting as the nonzero side force at a slip angle of zero, but it lacks a direct approach to measuring and modeling. The proposed measuring principle is to build quantitative relationships between ply steer and lateral acceleration.

Figure 1 shows a typical layout of an accelerometer-based intelligent tire developed by the authors. As shown in Figure 2, the lateral accelerations at different slip angles are also obtained. Two unusual phenomena that have never been reported are observed: (1) lateral accelerations demonstrate asymmetrical behavior with respect to left/right slip (Figure 2a), and (2) lateral accelerations at zero slip angle still exist and change along the circumference (Figure 2b). It is hypothesized that the underlying reasons for these two unusual phenomena are the ply steer–dependent kinematics and that they can conversely be used to measure the tire ply steer in situ. Furthermore, the accuracy of the intelligent tire's algorithm might be improved by suitable modeling of these observed phenomena. Previous researchers directly identify tire slip angle without considering this pseudoslip angle generated by ply steer. For example, Matsuzaki et al.[25] directly integrated lateral acceleration to obtain the lateral deformation of the tire tread. Hong et al.[26] used a differential form of the parabolic lateral deflection model to describe lateral acceleration without considering the special characteristics of lateral acceleration. Singh and Taheri[6] employed a line-fit algorithm for estimating the slip angle by simply calculating the magnitude of lateral acceleration. Systematic error might result if the influence of tire ply steer is not considered. The applicability of the slip angle prediction method may not be accurate enough.

Tires mostly work at small slip angles with constantly changing steering directions, which requires high robustness of the intelligent tire algorithm. Modeling the above two phenomena is the first step for accurate tire lateral parameter estimation. Therefore, the mixed Lagrange–Euler (MLE) approach for rolling contact kinematics is used to formulate the tire lateral acceleration, which links both rigid motion and elastic displacement. It is clearly found that the lateral acceleration is proportional to the square of the rotating velocity and the second-order gradient of displacement.

Downloaded from http://meridian.allenpress.com/rct/article-pdf/94/1/180/2807318/0035-9475-94-1-180.pdf by Ministry of Science and Technology (Thailand) user on 25 May 2022

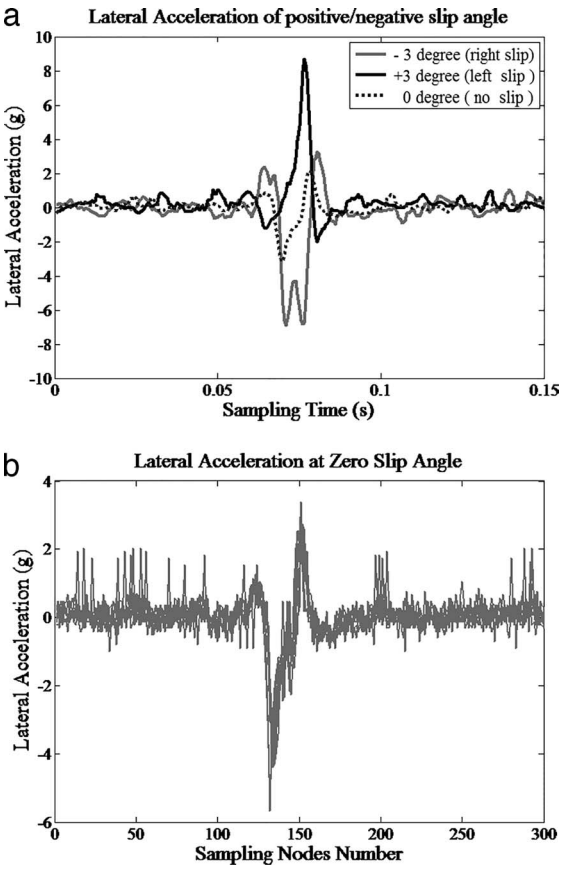

FIG. 2. — Lateral accelerations of zero slip angle and positive/negative slip angles.

Based on the analytical expression of acceleration as shown in Eq. 8, the unusual acceleration at zero slip angle can be naturally associated with ply steer, which manifests as the sinusoidal lateral deformation modes generated by the coupling of the bending-twist deformation of the cord–rubber composites of the tire belt. Although the coupling of the bending-twist deformation of the cord–rubber composites of the tire belt has been pointed out by previous researchers such as Walter,[27] Pottinger,[28,29] and Bert,[30] no kinematic model has been built to describe the lateral acceleration of tires while rolling. In this article, the influence of tire rolling is also considered to improve the physical model of ply steer.

The proposed hypothesis has been verified by finite element method (FEM) simulation and experimental results proving that tire ply steer leads to the observed unusual lateral acceleration pattern. Thus, the quantitative value of ply steer could be measured in situ by integrating the obtained lateral acceleration and, thus, the apparent elastic slip angle, even under zero external wheel slip angle. In this manner, the intelligent tire system provides a direct measuring and modeling approach for tire ply in motion. In addition, the accuracy of the intelligent tire's algorithm could be improved by suitable modeling of the asymmetrical acceleration and the tire slip angle estimation method based on consideration of ply steer in the intelligent tire.

In the first part of this article, an accelerometer-based intelligent tire system is introduced, and tire rolling kinematics are employed to obtain an analytical expression of acceleration fields. A tire ply steer deformation mechanism is also demonstrated through theoretical analysis. Then, the

Downloaded from http://meridian.allenpress.com/rct/article-pdf/94/1/180/2807318/0035-9475-94-1-180.pdf by Ministry of Science and Technology (Thailand) user on 25 May 2022

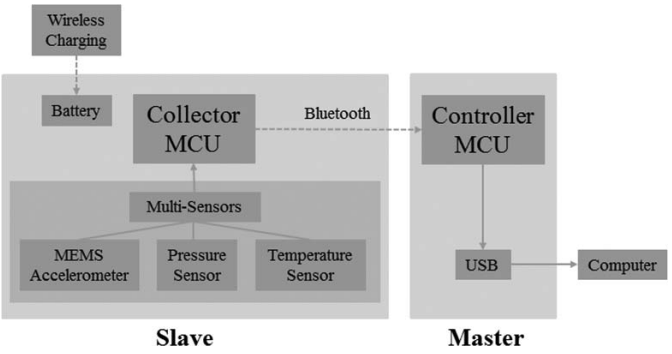

FIG. 3. — Intelligent tire system hardware architecture.

experimental design is described, followed by FEM simulation and comparison with the experimental results. Finally, the quantitative value of ply steer of a 205/55R16 tire is given using the proposed approach, demonstrating the validity and usefulness of the developed system.

INTELLIGENT TIRE SYSTEM

The purpose of this article is to develop an in situ measurement approach for tire ply steer based on a recently proposed accelerometer-based intelligent tire system. Thus, the hardware architecture of the developed intelligent tire system will be described first in this section. Then, the MLE approach is given to illustrate the relation between deformation and acceleration. Subsequently, the hypothesis that tire ply steer leads to nonzero and asymmetrical lateral acceleration is formulated.

INTELLIGENT TIRE HARDWARE SYSTEM AND EXPERIMENTS

The layout of the MEMS sensor-based intelligent tire system is shown in Figure 3 and consists of a MEMS accelerometer, pressure sensor, and temperature sensor, all fixed at the middle of the tire's inner liner. The sampling frequency is chosen as 2 kHz, which ensures that at least one set of data points can be collected for each 10 mm of rolling distance when the speed is less than 70 km/h. The entire system is composed of a collector and a controller. The sensors are fixed on the tire, while the collector microcontroller unit and rechargeable lithium battery are fixed on the hub. The measured data are transmitted wirelessly by Bluetooth to the controller and then the laptop. The signals can be checked in real time. The working power of the intelligent tire system is approximately 15 mW, which guarantees that the system can work for a relatively long period of time.

As shown in Figure 4a, the intelligent tire is instrumented to the MTS Flat-Trac Tire Test Systems to obtain the lateral accelerations of the tire at different slip angles, inflation pressures, and loads.

The obtained accelerations at zero wheel slip angle show distinctive characteristics: base values, peak values, amplitude of acceleration, and so on (Figure 4b). Intuitively, the base acceleration could contribute to rigid rotation, whereas peak values contribute to tire elastic deformation during tire–road interaction. The characteristics of radial and longitudinal accelerations are more straightforward and have been investigated by many previous researchers.[21–24] However, the characteristics of lateral accelerations have attracted less attention, and we observe two unusual phenomena of lateral acceleration that have never been noticed by previous research. (1) The actual lateral acceleration without side slip varies dramatically, and peak

Downloaded from http://meridian.allenpress.com/rct/article-pdf/94/1/180/2807318/0035-9475-94-1-180.pdf by Ministry of Science and Technology (Thailand) user on 25 May 2022

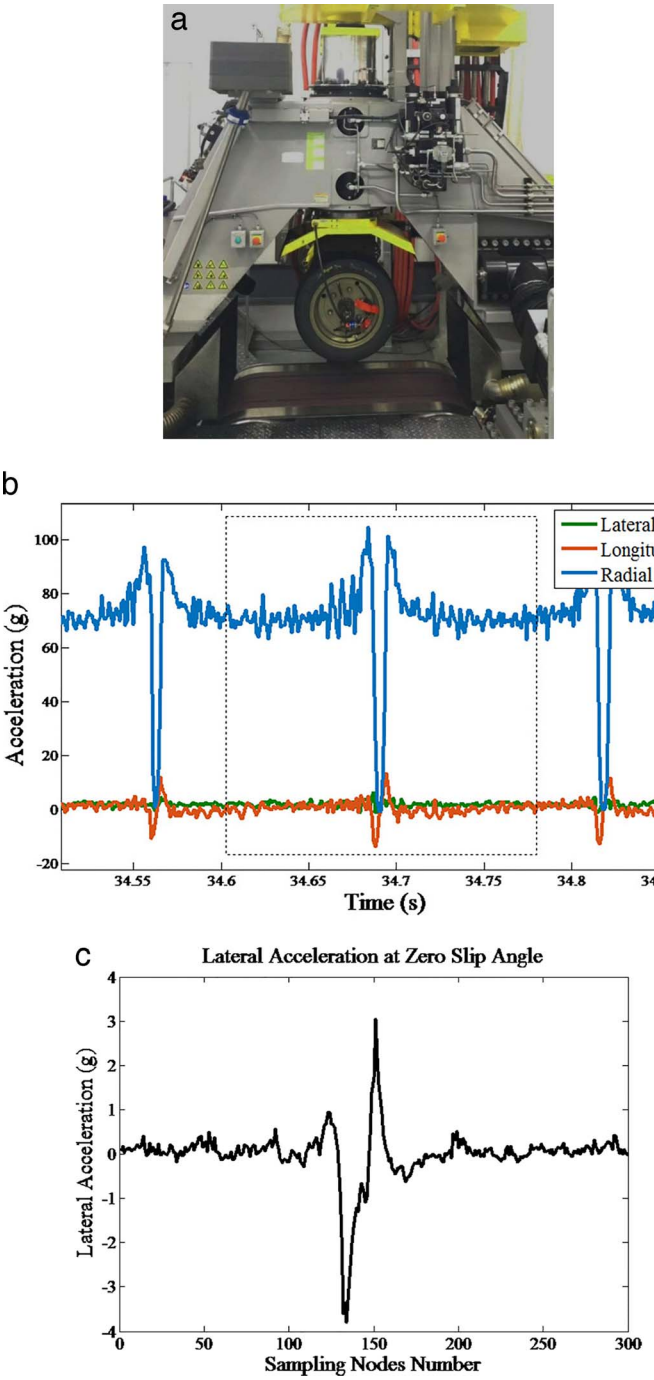

FIG. 4. — Intelligent tire system experiments: (a) MTS Flat-Trac tests; (b) three-axis accelerations; (c) lateral at zero slip angle.

Downloaded from http://meridian.allenpress.com/rct/article-pdf/94/1/180/2807318/0035-9475-94-1-180.pdf by Ministry of Science and Technology (Thailand) user on 25 May 2022

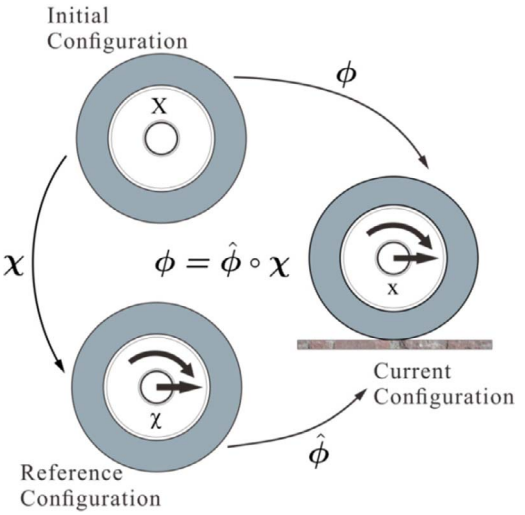

FIG. 5. — Mixed Lagrange–Euler method for decomposing the tire rolling contact.

values exist within the contact area (Figures 2b and 4c). (2) The lateral acceleration is not symmetrical, demonstrating that the characteristics of acceleration at positive and negative slip angles are different (Figure 2a). For positive slip angles, there is only one peak value. However, for negative slip angles, there are two peak values. This asymmetry of lateral acceleration has also never been observed or studied.

To explain the phenomenon, we first need to have a clear understanding of the acceleration generation mechanism, illustrating why lateral acceleration exhibits the above features. To this end, in the following section, the analytical expression of acceleration is given by using the MLE approach.

INTELLIGENT TIRE ACCELERATION EQUATION

In this section, the MLE approach originally developed by the authors' team for tire force and moment modeling is briefly introduced to deduce the intelligent tire kinematic equation.[31–35] Later, it will be shown that the kinematic formulation provides the theoretical foundation for the quantitative expression of ply steer.

As shown in Figure 5, the MLE method introduces a reference coordinate $\boldsymbol{\chi}$ between the Lagrangian coordinate $\mathbf{X}$ and the Eulerian coordinate $\mathbf{x}$, which separates the complex rolling movement of the tire into a pure rigid rotation motion and a pure tire rubber elastic deformation. The rigid rotation–reference configuration, which rotates at the same angular velocity as the structure, is defined to describe the motion of the rolling deformed tire.

Mapping $\mathbf{x} = \hat{\phi}(\boldsymbol{\chi},t)$ determines the position of point P at time t. Using the chain rule, the material velocity and acceleration can be deduced:

$$\mathbf{v} = \mathbf{v}(\hat{\phi}, t) = \mathbf{v}_0 + \left.\frac{\partial \hat{\phi}}{\partial t}\right|_X = \mathbf{v}_0 + \left.\frac{\partial \hat{\phi}}{\partial t}\right|_\chi + \nabla\hat{\phi} \cdot \mathbf{w} = \mathbf{v}_0 + \hat{\mathbf{v}} + \mathbf{v}_c,$$

$$\mathbf{a} = \mathbf{a}(\hat{\phi}, t) = \mathbf{a}_0 + \left.\frac{\partial^2 \hat{\phi}}{\partial t^2}\right|_X = \mathbf{a}_0 + \left.\frac{\partial^2 \hat{\phi}}{\partial t^2}\right|_\chi + \nabla(\nabla\hat{\phi} \cdot \mathbf{w}) \cdot \mathbf{w} = \mathbf{a}_0 + \hat{\mathbf{a}} + \mathbf{a}_c. \quad (1)$$

Downloaded from http://meridian.allenpress.com/rct/article-pdf/94/1/180/2807318/0035-9475-94-1-180.pdf by Ministry of Science and Technology (Thailand) user on 25 May 2022

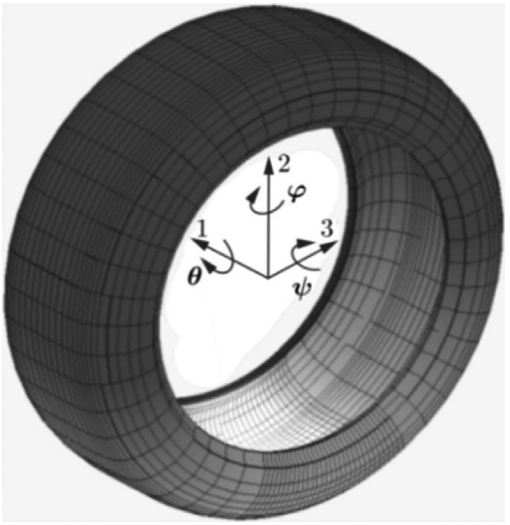

FIG. 6. — Definition of the reference coordinates system.

where $\mathbf{v}_0$ is the velocity of the rim center, $\hat{\mathbf{v}}$ is the relative velocity, $\mathbf{v}_c$ is the transport velocity, $\mathbf{a}_0$ is the acceleration of the rim center, $\hat{\mathbf{a}}$ is the relative acceleration, $\mathbf{a}_c$ is the transport acceleration, and $\mathbf{w}$ is the rotation velocity of a rigid body.

At steady-state conditions, the accelerations are not functions of time; therefore, the relative acceleration is zero. Letting $\mathbf{u} = \mathbf{x} - \boldsymbol{\chi}$, the steady-state acceleration can be written as

$$\mathbf{a}(\chi) = \mathbf{a}_0 + \nabla\Big((\nabla\mathbf{u} + \mathbf{I}) \cdot \mathbf{w}\Big) \cdot \mathbf{w}. \tag{2}$$

where $\mathbf{u}$ is the elastic deformation and $\mathbf{I}$ is the unit matrix. As shown in Figure 6, the Euler angle is introduced to describe the complex rolling motion of the tire with side slip and rollover:

$$\theta^w = [\psi\ \varphi\ \theta]^T, \tag{3}$$

where ψ is the camber angle, φ is the slip angle, and θ is the rotating angle. Equations 1, 2, and 3 correspond to the lateral, radial, and rolling directions of the tire, respectively. The accelerometer is fixed in the middle of the tire's inner liner, which means that it moves along with the tire, and therefore, the angular velocity should be described in the wheel coordinate system as follows:

$$\mathbf{w} = \begin{bmatrix} 0 & -\bar{\omega}_3 & \bar{\omega}_2 \\ \bar{\omega}_3 & 0 & -\bar{\omega}_1 \\ -\bar{\omega}_2 & \bar{\omega}_1 & 0 \end{bmatrix} \cdot \begin{bmatrix} \chi_1 \\ \chi_2 \\ \chi_3 \end{bmatrix}, \tag{4}$$

$$\bar{\omega}_1 = -\frac{d\psi}{dt}\sin\varphi + \frac{d\theta}{dt},$$

$$\bar{\omega}_2 = \frac{d\psi}{dt}\cos\psi\sin\theta + \frac{d\varphi}{dt}\cos\theta,$$

$$\bar{\omega}_3 = \frac{d\psi}{dt}\cos\psi\cos\theta - \frac{d\varphi}{dt}\sin\theta. \tag{5}$$

where $\bar{\omega}_1$,$\bar{\omega}_2$,$\bar{\omega}_3$ denote the angular velocity in the three directions.

Downloaded from http://meridian.allenpress.com/rct/article-pdf/94/1/180/2807318/0035-9475-94-1-180.pdf by Ministry of Science and Technology (Thailand) user on 25 May 2022

Generally, the camber angle is fixed, leading to $d\psi/dt = 0$. In addition, the change rate of the side-slip angular velocity is very small when compared with the rotational angular velocity, leading to $d\varphi/dt \approx 0$. The steady-state rotation velocity is $d\theta/dt = \Omega$. This article mainly focuses on the lateral deformation and kinematics, so the lateral acceleration can be deduced by substituting Eqs. 4 and 5 for Eq. 2.

$$a_1 = u_{1,22}\chi_3^2 + u_{1,33}\chi_2^2 - u_{1,32}\chi_2\chi_3 - u_{1,23}\chi_2\chi_3 - u_{1,2}\chi_2 - u_{1,3}\chi_3, \tag{6}$$

where $u_{i,j}$ and $u_{i,jk}$ are the first- and second-order elastic displacement gradients, respectively. Considering that the tire deformation can be represented in cylindrical coordinates, it satisfies the equation

$$\frac{D^2u_k}{D\theta^2} = u_{k,22}\chi_3^2 + u_{k,33}\chi_2^2 - u_{k,32}\chi_2\chi_3 - u_{k,23}\chi_2\chi_3 - u_{k,2}\chi_2 - u_{k,3}\chi_3. \tag{7}$$

Therefore, the lateral acceleration can be simplified as

$$a_1 = \Omega^2 \frac{d^2u_1}{d\theta^2}. \tag{8}$$

Similarly, the radial and longitudinal acceleration can be calculated as

$$a_2 = \Omega^2 \frac{d^2u_2}{d\theta^2},\ a_3 = \Omega^2 \frac{d^2u_3}{d\theta^2}. \tag{9}$$

It can be seen that the acceleration obtained by the sensors is the consequence of tire rigid-flexible coupling motion. Equations 8 and 9 provide a simple method for calculating acceleration fields, which demonstrates that (1) the amplitude of acceleration is proportional to the square of rolling speed and (2) the waveform variation of acceleration is related to the second-order derivative of the elastic deformation in the three directions. Therefore, the characteristic of lateral acceleration is associated with the lateral elastic deformation module.

According to the acceleration at zero slip angle and the acceleration equation, it can be inferred that the nonzero lateral acceleration at zero slip angle is generated by the nonzero lateral elastic deformation, which is hypothesized to be the tire ply steer kinematics. Ply steer is mainly induced by the composite mechanics of tire belt structures, as shown in Figure 7. When the tire body is subjected to vertical load, the bending-twisting coupling deformation will be generated, manifesting as pseudoslip angle and ply steer force. It is this bending-twisting coupling deformation that generates pseudoslip angle and lateral deformation and finally is presented in the form of acceleration signal during rolling.

TIRE PLY STEER: HYPOTHESIS, VERIFICATION AND MEASUREMENT

From Eq. 8, it is clear that lateral acceleration is associated with lateral deformation at zero slip angle, which is the lateral deformation caused by ply steer. Therefore, the characteristics of lateral acceleration can be explained only by accurately characterizing the deformation mode of ply steer.

There has been some work conducted by Walter,[27] Pottinger,[28,29] and Bert[30] to illustrate the ply steer phenomenon. They attributed tire ply steer to the bending-twisting coupling relationship.

However, the existing hypothesis considers only the pure static state and neglects that ply steer is a rolling contact phenomenon. Actually, lateral force will not be generated unless there is rolling velocity. Therefore, study of the ply steer phenomenon should look further to the tire rolling kinematics on the basis of existing composite material mechanical tire models.

Downloaded from http://meridian.allenpress.com/rct/article-pdf/94/1/180/2807318/0035-9475-94-1-180.pdf by Ministry of Science and Technology (Thailand) user on 25 May 2022

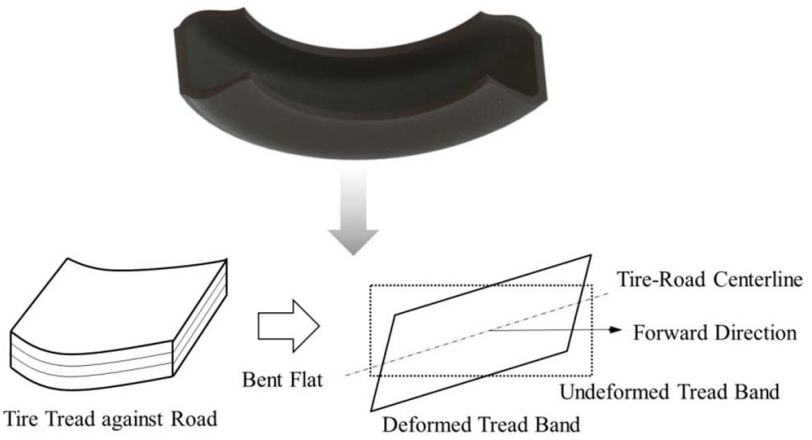

FIG. 7. — Distortion of tire rubber against road.

PLY STEER HYPOTHESIS THEORY FOR LATERAL ACCELERATION

In this section, tire ply steer generation theory will be demonstrated by coupling tire static contact deformation and tire rolling kinematics. As shown in Figure 8a, a tire is a composite structure consisting of different components. A two-dimensional model of the tire will be simulated by the FEM. When several laminas are assembled to form a laminate, the anisotropy and interaction between laminas will lead to bending-twisting coupling behavior in the laminate.[36–40]

The laminate constitutive relation can be written as

$$\begin{bmatrix} N_x \\ N_y \\ N_{xy} \\ M_x \\ M_y \\ M_{xy} \end{bmatrix} = \begin{bmatrix} A_{11} & A_{12} & A_{16} & B_{11} & B_{12} & B_{16} \\ A_{21} & A_{22} & A_{26} & B_{21} & B_{22} & B_{26} \\ A_{61} & A_{62} & A_{66} & B_{61} & B_{62} & B_{66} \\ B_{11} & B_{12} & B_{16} & D_{11} & D_{12} & D_{16} \\ B_{21} & B_{22} & B_{26} & D_{21} & D_{22} & D_{26} \\ B_{61} & B_{62} & B_{66} & D_{61} & D_{62} & D_{66} \end{bmatrix} \begin{bmatrix} \varepsilon_x^0 \\ \varepsilon_y^0 \\ \gamma_{xy}^0 \\ k_x \\ k_y \\ k_{xy} \end{bmatrix}, \tag{10}$$

where the rolling direction is denoted by x and the lateral direction is denoted by y; N_x, N_y, N_{xy}, M_x, M_y, and M_{xy} are the internal forces and moments along different directions; ε_x^0, ε_y^0, γ_{xy}^0, k_x, k_y, and k_{xy} are midplane strains and curvatures separately; and A_{ij}, B_{ij}, and D_{ij} denote the material properties of the laminate specified in the Appendix.

The materials of each lamina (rubber, nylon, steel, etc.) differ from one another. However, the modulus of the steel belt is largest and dominates the property of the laminate. Thus, the steel belt is the primary focus. As shown in Figure 8b, the steel belt of the tire is arranged symmetrically. It is assumed that the thickness of each layer of the belt is equal, which means that the cord angles are arranged in the order +δ/–δ. Thus, it can be deduced that

$$A_{16} = A_{26} = 0. \tag{11}$$

Under vertical force without side slip, the tire could be considered to be subjected to a pure bending along the rolling direction (x direction). Thus, the in-plane shear force relative to the x, y axes is almost zero, and there is little bending curvature change in the y axis or twisting curvature change, which means that

Downloaded from http://meridian.allenpress.com/rct/article-pdf/94/1/180/2807318/0035-9475-94-1-180.pdf by Ministry of Science and Technology (Thailand) user on 25 May 2022

FIG. 8. — Structure of tire: (a) structure and material; (b) symmetrical tire steel belt.

$$N_{xy} = 0,\ k_y = 0, k_{xy} = 0. \tag{12}$$

Using the third column of Eq. 10 it can be obtained that

$$A_{66}\gamma^0_{xy} + B_{61}k_x = 0. \tag{13}$$

where the midplane shear strain ε_{xy} can be expressed as

$$\gamma^0_{xy} = \frac{1}{2}\left(\frac{\partial v_y}{\partial x} + \frac{\partial u_x}{\partial y}\right). \tag{14}$$

Meanwhile, according to classical linear elasticity theory, the bending-twisting angle can be expressed as

$$\phi_z = \frac{1}{2}\left(\frac{\partial v_y}{\partial x} - \frac{\partial u_x}{\partial y}\right). \tag{15}$$

where u_x, v_y are the displacements in the x–, y– directions. For the ply steer condition, the deformation is mainly caused by lateral displacement. The displacement in rolling direction can be

Downloaded from http://meridian.allenpress.com/rct/article-pdf/94/1/180/2807318/0035-9475-94-1-180.pdf by Ministry of Science and Technology (Thailand) user on 25 May 2022

neglected compared with the lateral direction, that is,

$$\frac{\partial u_x}{\partial y} = 0. \tag{16}$$

Thus, the bending-twisting angle is finally obtained

$$\phi_z = \frac{1}{2}\frac{\partial v_y}{\partial x} = \frac{1}{2}\gamma_{xy}^0. \tag{17}$$

Substituting Eq. 13 into Eq. 17, it can be obtained that

$$\phi_z = -\frac{1}{2}k_x\left(\frac{B_{16}}{A_{66}}\right). \tag{18}$$

Although the coupling of the bending-twist deformation of the cord–rubber composites of the tire belt has been pointed out by previous researchers such as Walter,[27] Pottinger,[28,29] and Bert,[30] no kinematic model has been built to describe the lateral acceleration of a tire while rolling, which is the focus of this article.

According to the MLE approach,[30–34] the differential integral equations of the contact kinematics can be written as

$$\frac{\partial \bar{u}_1}{\partial \bar{z}}\mathbf{v}_T + \frac{\partial \bar{u}_1}{\partial t} = \mathbf{v}_1(\chi). \tag{19}$$

where $\bar{u}_1$ denotes the lateral deformation of the tire tread, $\bar{z}$ denotes the position in longitudinal direction of the contact region, $\mathbf{v}_T$ is the transport velocity of the tire tread moving through the contact area, and $\mathbf{v}_1$ is the lateral slip velocity of the tire belt. At the steady state, we have $\partial \bar{u}_1/\partial t = 0$. The lateral velocity can be written as

$$\mathbf{v}_1(\chi) = -\Omega\chi_3 u_{1,2} + \Omega\chi_2 u_{1,3}, \tag{20}$$

where $u_{1,2}$ can be neglected compared with $u_{1,3}$. In addition, $u_{1,3} = \partial v_y/\partial x$, which is caused by the bending-twisting angle ϕ_z. It is clear from Eq. 20 that the bending-twisting coupling characteristic leads to the slip velocity of the tire belt in the lateral direction. Then, according to Eq. 19, the velocity of the tire belt will induce the deformation of the tire tread $\bar{u}_1$ against the road in the contact area.

The tire tread can be assumed as a group of brushes with stiffness. Therefore, the lateral force could be obtained by $F_1 = \int_L^T c_1\bar{u}_1$, where c_1 denotes the lateral stiffness of the tire tread brush and L and T correspond to the leading and trailing edge of the contact region, respectively.

From the above equation, it can be seen that the final deformation is caused by both the static bending-twisting coupling deformation and tire rolling. In summary, the generation of ply steer and intelligent tire acceleration signals under ply steer are demonstrated via the following steps:

Step 1: At pure static vertical load, the composite laminate properties leads to bending-twisting coupling deformation in the contact region, that is, the twisting angle $\phi_z = -1/2\ k_x\ (B_{16}/A_{66})$.

Step 2: After the tire is rolling, the longitudinal rolling velocity will lead to tire tread lateral velocity because of the twisting angle: $\partial \bar{u}_1/\partial \bar{z}\mathbf{v}_T = \Omega\chi_2 u_{1,3}$.

Step 3: The lateral velocity will generate lateral deformation and finally lateral force. The lateral force exists when there is no steer angle, and it is the combination of tire rolling and static deformation.

Step 4: The lateral deformation induces the lateral acceleration: $a_1 = \Omega^2(d^2u_1/d\theta^2)$. The ply steer acceleration will eventually lead to the asymmetry of acceleration at side slip.

Downloaded from http://meridian.allenpress.com/rct/article-pdf/94/1/180/2807318/i0035-9475-94-1-180.pdf by Ministry of Science and Technology (Thailand) user on 25 May 2022

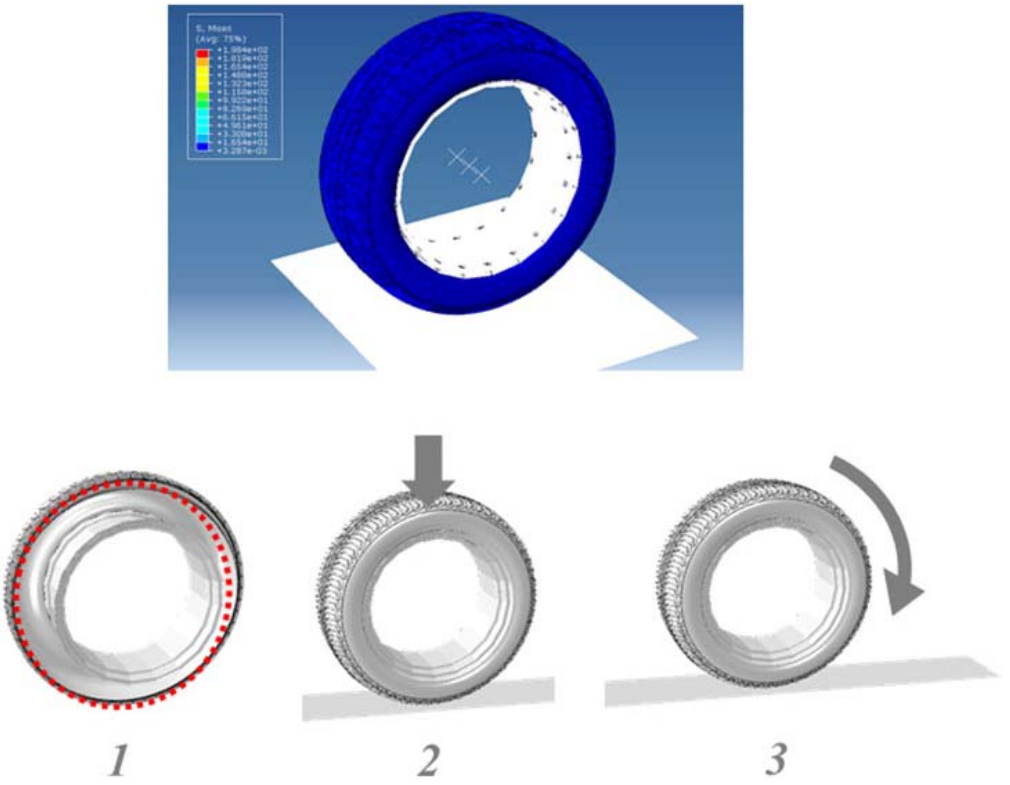

FIG. 9. — ABAQUS tire model simulation.

SIMULATION AND EXPERIMENTAL VALIDATION

The above analysis has illustrated ply steer deformation and proposed the hypothesis of lateral acceleration. To validate the improved ply steer theory and acceleration generation hypothesis, FEM simulations are adopted. A 205/55R16 passenger car tire model is established. The tire is subjected to 2.5 bar pressure, 400 kg vertical force, and rolling at speed of 60 km/h. The lateral deformations of a streamline of nodes in the center of the tire are extracted. As shown in Figure 9, the simulation is composed of two steps. First, a vertical load is applied until the tire is at equilibrium. After that, a steady rolling velocity is given.

The lateral deformations of the two steps are depicted in Figure 10. The deformation results agree with the above proposed ply steer theory:

1. The lateral displacement at pure vertical load presents a sinusoidal waveform. Within the contact area, the lateral displacement causes a pseudoslip angle, corresponding to the bending-twisting coupling angle.
2. After the tire is rolling, the lateral deformation is mainly oriented to one side. Within the contact region, the lateral deformation exhibits a slight convex–concave behavior, which may be caused by the static sinusoidal deformation.
3. The difference of lateral deformation between the static and the rolling condition is depicted, which is similar to the deformation when a concentrated force is exerted.

Downloaded from http://meridian.allenpress.com/rct/article-pdf/94/1/180/2807318/0035-9475-94-1-180.pdf by Ministry of Science and Technology (Thailand) user on 25 May 2022

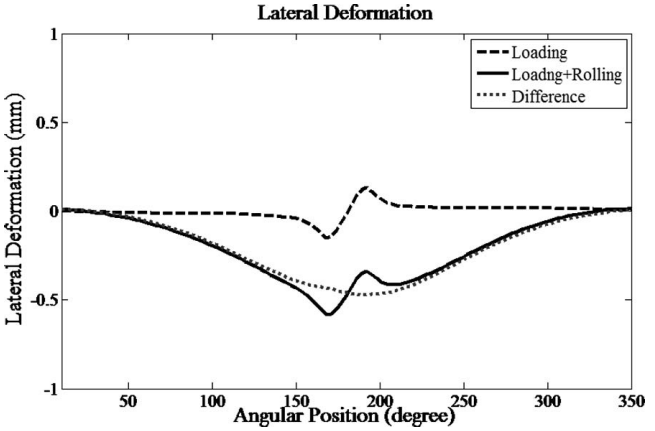

FIG. 10. — Lateral displacement of the tire central nodes.

The simulation results fully demonstrate the changing process of lateral deformation: twisting deformation at static state, lateral force generation during tire rolling, and final stable lateral deformation. The lateral deformation confirms the above theoretical hypothesis that ply steer is a comprehensive result of composite-material mechanics and tire rolling kinematics.

Although the contact transient process is not captured in the finite element solution, leading to inaccurate contact deflection of the tire, it can still be found that the simplified parabolic curve is not sufficient to describe the complex lateral deformation.

With the above analytical equation of lateral acceleration and the simulated lateral deformation results, the lateral acceleration can be obtained. The lateral acceleration under the same condition is also measured for comparison with the calculated acceleration.

As shown in Figure 11, the measured and simulated accelerations at zero slip angle match well with each other, which validates the hypothesis that tire ply steer is the main reason for nonzero lateral acceleration without sides lip. At different slip directions, the ply steer–caused acceleration is superposed on the slip-caused acceleration, which explains why the acceleration under left/right slip is asymmetric.

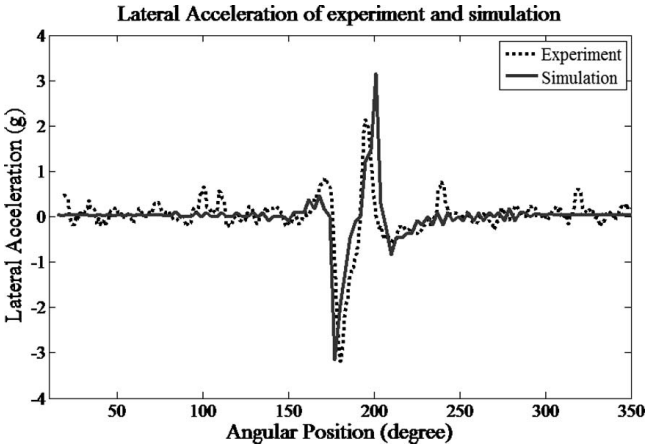

FIG. 11. — Comparison of lateral acceleration between simulation results with experimental results.

Downloaded from http://meridian.allenpress.com/rct/article-pdf/94/1/180/2807318/0035-9475-94-1-180.pdf by Ministry of Science and Technology (Thailand) user on 25 May 2022

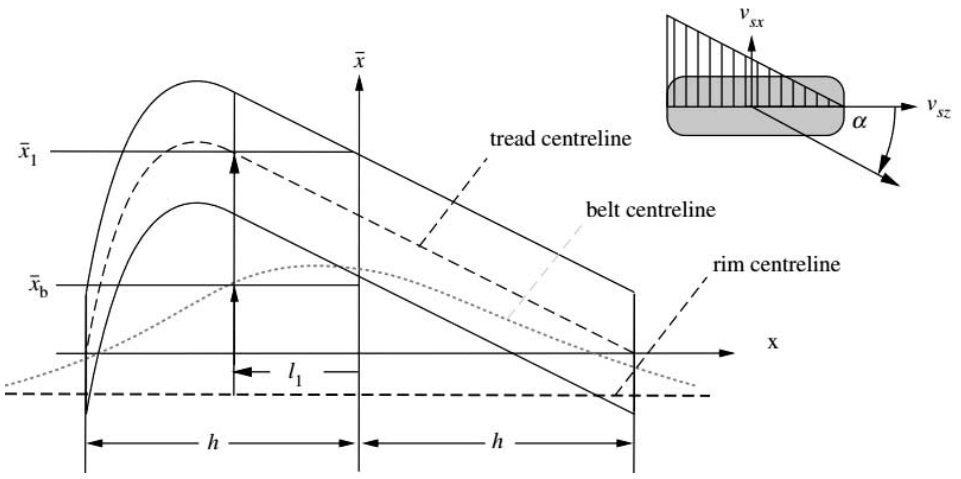

FIG. 12. — Fila tire model.[31]

PLY STEER MEASUREMENT BY INTELLIGENT TIRE

The proposed hypothesis has been validated by the FEM simulation and experimental results, proving that tire ply steer leads to the observed unusual lateral acceleration pattern. Thus, the quantitative value of ply steer could be measured in situ by integrating the obtained lateral acceleration, and thus the apparent elastic slip angle, at less than zero external wheel slip angle.

Because acceleration is proportional to the second-order derivative of the deformation, a slight change of deformation will be amplified in the acceleration signal. More details can be found by integrating the acceleration signal back to the original deformation as

$$u_1 = \frac{\iint a_1 \mathrm{d}\theta \mathrm{d}\theta}{\Omega^2}. \tag{21}$$

To describe elastic ply steer deformation and the extent of elastic pseudosteer, the ply steer angle is redefined rather than using the bending-twisting angle as the ply steer angle as in the literature.[27–30]

For the Fiala model, the contact region is divided into two parts, as shown in Figure 12. In the first part, there is no relative slip between tire and ground, and in the second part, there is relative slip. The slope of the first part corresponds to the side-slip angle. Similar to the slip angle definition in the Fiala tire model, the slope of lateral deformation near the leading edge of the tire–road contact is applied to describe the ply steer angle, as shown in Figure 12. The lateral deformation in Figure 13 is obtained by integration of the experimental lateral acceleration.

Based on the proposed ply steer angle definition, the intelligent tire system could provide a direct method for monitoring tire ply steer. In particular, it must be pointed out that the intelligent tire's in situ measurement of ply steer is the first step in measuring other lateral parameters of the tire.

First, the asymmetric lateral acceleration is associated with ply steer, so the slip direction can be confirmed by the characteristic of lateral acceleration. Second, by subtracting only the pseudosteer elastic deformation, the actual deformation caused by the external wheel slip angle can be determined accurately. Furthermore, the accuracy of the intelligent tire's algorithm might be improved because the commonly occurring ply steer for radial tires is well modeled and monitored by the proposed approach.

Downloaded from http://meridian.allenpress.com/rct/article-pdf/94/1/180/2807318/0035-9475-94-1-180.pdf by Ministry of Science and Technology (Thailand) user on 25 May 2022

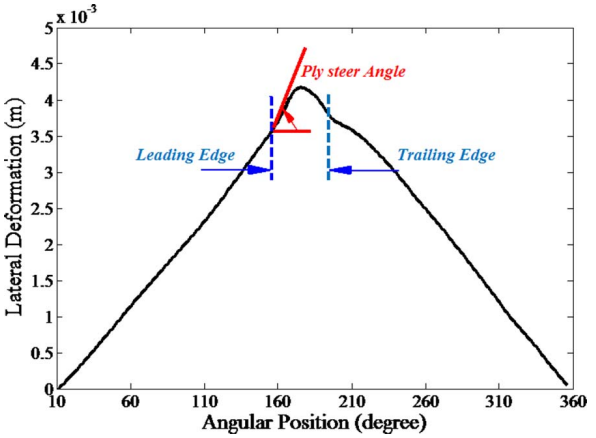

FIG. 13. — Lateral deformation integrated and ply steer angle.

According to the above described method, the lateral deformation and defined ply steer angle of a 205/55R16 passenger tire at different conditions are calculated to determine the influencing factors of ply steer, as shown in the following tables and figures.

From the monitored ply steer angle results by the proposed intelligent tire in situ measurement method, the following can be observed:

1. Ply steer angle is more sensitive to tire pressure than vertical load. With increasing tire pressure, the ply steer angle decreases. With increasing vertical load, the ply steer angle slightly increases.
2. As shown in Figure 14 and Table I, the trend of ply steer with tire pressure monitored by the intelligent tire agrees well with that of previous experiments (i.e., the ply steer decreases with increasing tire pressure).[41]
3. As shown in Figure 15 and Table II, the trend of ply steer with vertical load monitored by the intelligent tire agrees well with that of our own experiments (i.e., the ply steer increases with increasing tire load). Therefore, it is safe to say that the feasibility of monitoring the tire ply steer angle by an intelligent tire has been validated.
4. According to the theoretical analysis, the bending-twisting angle is related to the bending-shearing coupling stiffness B_{16}, the in-plane shearing stiffness A_{66}, and the curvature change of the tire contact area k_x. When the tire pressure increases, the vertical stiffness of the tire becomes larger, leading to a smaller contact area, which means that the curvature change k_x is smaller. Therefore, the extent of ply steer is less severe. Similarly, the increasing vertical load will intensify the extent of ply steer.

The above results show the capability of intelligent tire monitoring of the tire ply steer condition, and the extent of elastic lateral deformation without side slip can also be demonstrated well by the defined ply steer angle.

CONCLUSION

This article has proposed a method for in situ monitoring of tire ply steering based on an intelligent tire system. Through experiments and theoretical analysis, several points can be concluded:

Downloaded from http://meridian.allenpress.com/rct/article-pdf/94/1/180/2807318/0035-9475-94-1-180.pdf by Ministry of Science and Technology (Thailand) user on 25 May 2022

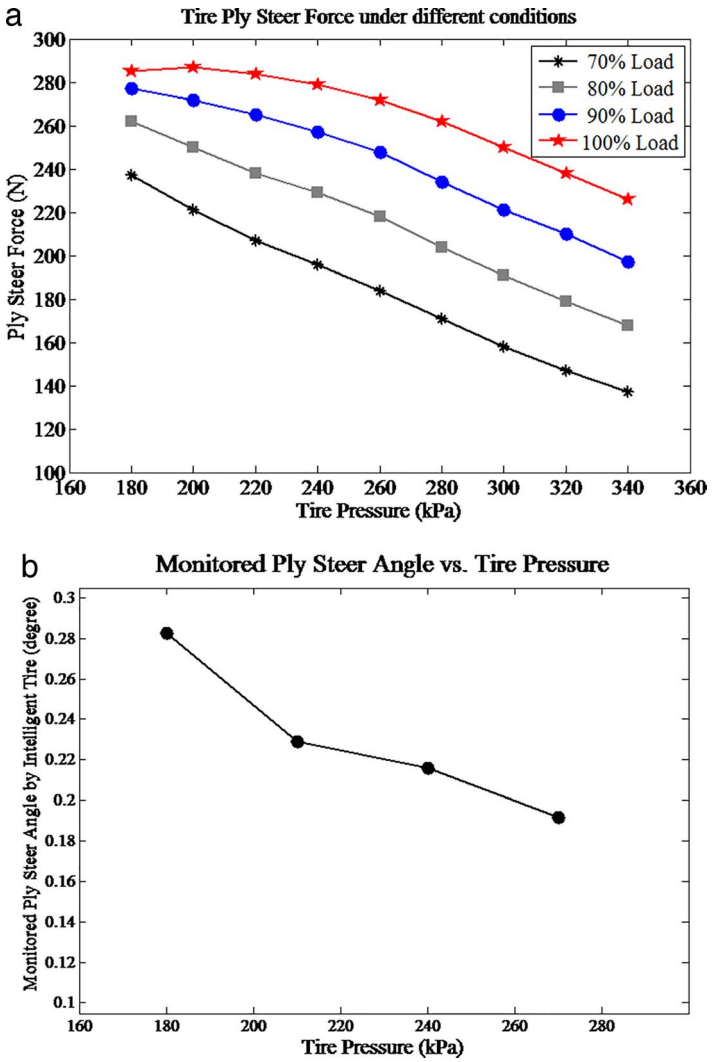

FIG. 14. — Relation between monitored ply steer angle and measured lateral force at different tire pressures: (a) tire pressure vs ply steer force from the literature; (b) tire pressure vs monitored ply steer angle.

- The developed accelerometer-type intelligent tire system was established, which provides a new tool for estimating tire dynamic parameters. The acceleration signal is the core of the estimation algorithm. Through the equation of tire rolling kinematics, it can be observed that the measured acceleration is related to the second-order derivative of the lateral

TABLE I
PLY STEER ANGLE UNDER DIFFERENT TIRE PRESSURES

	Tire condition: tire pressure, bar			
	1.8	2.1	2.4	2.7
Monitored ply steer angle, °	0.2826	0.229	0.2159	0.1916

Downloaded from http://meridian.allenpress.com/rct/article-pdf/94/1/180/2807318/0035-9475-94-1-180.pdf by Ministry of Science and Technology (Thailand) user on 25 May 2022

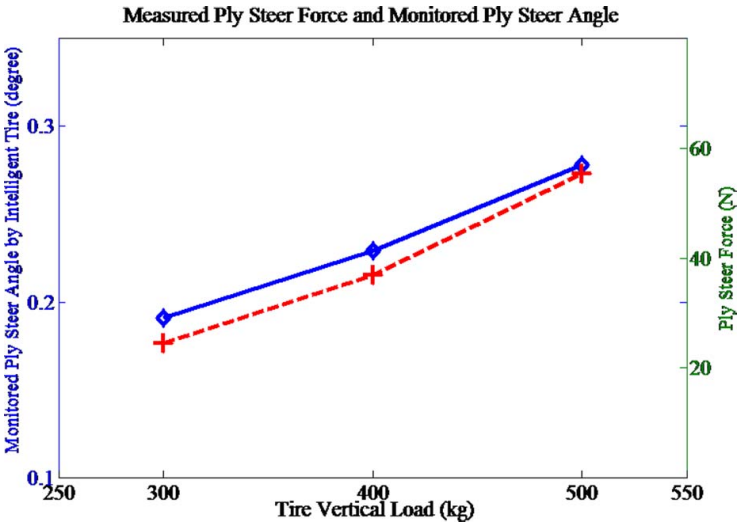

FIG. 15. — Relation between monitored ply steer angle and measured lateral force under different vertical loads.

deformation and tire rigid rolling velocity. The acceleration analytic expression was first proposed, which is the theoretical foundation for intelligent tire research.

- Because of the ply steer of the tire, lateral deformation presents a sinusoidal curve at vertical force, which results in a bending-twisting angle. Based on tire rolling kinematics, the twisting angle at rolling velocity leads to tire tread lateral velocity and eventually a lateral deformation. The lateral force without slip angle is generated this way. This also provides a perfect explanation for why the lateral force direction changes with tire rolling direction.
- Because of tire ply steer, the lateral acceleration of the intelligent tire still changes without side slip. The feature of lateral acceleration is not symmetric at positive and negative slip angles because of the original ply steer.
- The proposed ply steer angle is a definition of the extent of ply steer. For a 205/55R16 passenger tire, the ply steer angle is approximately 0.2° and changes with different working conditions. The ply steer angle increases with decreasing tire pressure and increasing vertical load, which is in agreement with the theoretical conclusion.
- The algorithm for estimating the lateral properties of a tire using the intelligent tire system is based on lateral acceleration. However, the true lateral acceleration signal related to lateral force is combined with other distractors. Thus, accurate prediction of the ply steer angle by the intelligent tire is the foundational work for the slip angle, lateral force prediction, and further intelligent tire applications.

TABLE II
PLY STEER ANGLE UNDER DIFFERENT VERTICAL LOADS

	Tire condition: vertical load, kg		
	300	400	500
Monitored ply steer angle, °	0.1907	0.229	0.2781
Measured ply steer force, N	24.39	36.89	55.44

Downloaded from http://meridian.allenpress.com/rct/article-pdf/94/1/180/2807318/0035-9475-94-1-180.pdf by Ministry of Science and Technology (Thailand) user on 25 May 2022

In summary, the intelligent tire system provides a practical approach for calculating tire ply steer angle, which is significant for the research of both the tire ply steer mechanism and intelligent tire applications.

ACKNOWLEDGEMENT

The authors would like to acknowledge the financial support provided by the National Natural Science Foundation of China (No. 51761135124 and No. 11672148), German Research Foundation (No. KA M63/42), Tsinghua University Fund (No.2018Z05JZY014), and the State Key Laboratory Fund of Automotive Safety and Energy throughout this research.

REFERENCES

[1]F. Braghin, M. Brusarosco, F. Cheli, A. Cigada, S. Manzoni, and F. Mancosu, *Veh. Syst. Dyn*. **44**, 3 (2006).

[2]A. J. Tuononen, *Sensors* **9**, 8761 (2009).

[3]A. J. C. Schmeitz and A. P. Teerhuis, *Tire Sci. Technol*. **46**, 105 (2018).

[4]M. A. Arat, K. B. Singh, and S. Taheri, *Int. J. Veh. Des*. **65**, 118 (2014).

[5]S. Hong, G. Erdogan, K. Hedrick, and F. Borrelli, *Veh. Syst. Dyn*. **51**, 627 (2013).

[6]K. B. Singh and S. Taheri, *Syst. Sci. Control Eng*. **3**, 39 (2015).

[7]V. D'Alessandro, S. Melzi, M. Sbrosi, and M. Brusarosco, *Veh. Syst. Dyn*. **50**, 3 (2012).

[8]M. Brusarosco, A. Cigada, and S. Manzoni, *Veh. Syst. Dyn*. **49**, 855 (2011).

[9]P. Behroozinia, S. Taheri, and R. Mirzaeifar, *Mech. Based Des. Struct. Mech*. **46**, 168 (2018).

[10]A. Tuononen, *Int. J. Heavy Veh. Syst*. **16**, 362 (2009).

[11]A. J. Tuononen, *Veh. Syst. Dyn*. **46**, 471 (2008).

[12]Y. Xiong and A. Tuononen, *J. Terramech*. **61**, 33 (2015).

[13]R. Matsuzaki, A. Todoroki, H. Kobayashi, and Y. Shimamura, *Adv. Compos. Mater*. **14**, 147 (2005).

[14]R. Matsuzaki and A. Todoroki, *Sens. Actuator A Phys*. **126**, 277 (2006).

[15]R. Matsuzaki and A. Todoroki, *Sens. Actuator A Phys*. **119**, 323 (2005).

[16]A. Todoroki, S. Miyatani, and Y. Shimamura, *Smart Mater. Struct*. **12**, 403 (2003).

[17]Y. Zhang, J. Yi, and T. Liu, *IEEE Sens. J*. **13**, 1756 (2013).

[18]R. Matsuzaki, T. Keating, A. Todoroki, and N. Hiraoka, *Sens. Actuator A Phys*. **148**,1 (2008).

[19]L. Hojong, M. T. Kim, and S. Taheri, *Tire Sci. Technol*. **46**, 276 (2018).

[20]O. Yilmazoglu, M. Brandt, J. Sigmund, E. Genc, H. L. Hartnagel, *Sens. Actuator A Phys*. **94**, 59 (2001).

[21]M. Matilainen and A. Tuononen, *Mech. Syst. Signal Proc*. **52**, 548 (2015).

[22]M. Brusarosco, A. Cigada, and S. Manzoni, *Veh. Syst. Dyn*. **46**, 1013 (2008).

[23]G. Erdogan, F. Borrelli, R. Tebano, G. Audisio, G. Lori, and J. Sannazzaro, "Development of a New Lateral Stability Control System Enhanced with Accelerometer Based Tire Sensors," presented at the ASME 2010 Dynamic Systems and Control Conference, Cambridge, MA, September 1215, 2010

[24]A. J. Niskanen and A. J. Tuononen, *Veh. Syst. Dyn*. **52**, 287 (2014).

[25]R. Matsuzaki, K. Kamai, and R. Seki, *Smart Mater. Struct*. **24**, 2 (2015).

[26]S. Hong, G. Erdogan, K. Hedrick, and F. Borrelli, *Veh. Syst. Dyn*. **51**, 627 (2013).

[27]J. D. Walter, RUBBER CHEM. TECHNOL. **51**, 524 (1978).

[28]M. G. Pottinger, "Ply Steer in Radial Carcass Tires," presented at the SAE International 1976 Automobile Engineering Meeting, 1976.

[29]M. G. Pottinger, U.S. Patent 3,945,422 (to B.F. Goodrich Co.), March 23, 1976.

[30]C. W. Bert, *Tire Sci. Technol*. **8**, 3 (1980).

Downloaded from http://meridian.allenpress.com/rct/article-pdf/94/1/180/2807318/0035-9475-94-1-180.pdf by Ministry of Science and Technology (Thailand) user on 25 May 2022

[31]C. Oertel and Y. T. Wei, *Veh. Syst. Dyn*. **50**, 1673 (2012).

[32]Y. T. Wei, C. Oertel, and X. Shen, *Veh. Syst. Dyn*. **50**, 1689 (2012).

[33]Y. T. Wei, C. Oertel, Y. Liu, and X. Li, *Veh. Syst. Dyn*. **54**, 20 (2016).

[34]Y. T. Wei, C. Oertel, X. Li, and L. Yu, *Proc. Inst. Mech. Eng. Part D* **231**, 1461 (2017).

[35]T. Berger, R. Behnke, and M. Kaliske, RUBBER CHEM. TECHNOL. **89**, 499 (2016).

[36]MR. Gurvich, RUBBER CHEM. TECHNOL. **79**, 217 (2006).

[37]MR. Gurvich, RUBBER CHEM. TECHNOL. **80**, 608 (2007).

[38]X. S. Yi, S. Du, and L. Zhang, Eds., "An Introduction to Composite Materials," in *Composite Materials Engineering*, Springer, Singapore, 2018.

[39]S. K. Clark, *Text. Res. J*. **33**, 295 (1963).

[40]G. Buytaert, F. Coornaert, and W. Dekeyser, RUBBER CHEM. TECHNOL. **82**, 430 (2009).

[41]C. Liu, Z. G. Liu, X. F. Zhang, T. Q. Du, and C. Tian, *China Rubber Industry* **1**, 3 (2019).

[*Received September 2019, Revised December 2019*]

Downloaded from http://meridian.allenpress.com/rct/article-pdf/94/1/180/2807318/0035-9475-94-1-180.pdf by Ministry of Science and Technology (Thailand) user on 25 May 2022

APPENDIX
Notation

$\mathbf{X}$, $\boldsymbol{\chi}$, $\mathbf{x}$	Lagrange coordinates, reference coordinates, and Eulerian coordinates
$\hat{\phi}(\boldsymbol{\chi})$	Mapping from reference coordinates to Eulerian coordinates
$\phi(\mathbf{X})$	Mapping from Lagrange coordinates to the Eulerian coordinates
$\boldsymbol{\chi}(\mathbf{X})$	Mapping from Lagrange coordinates to reference coordinates
$\mathbf{a}$	Acceleration of the reference point
$\mathbf{a}_0$	Acceleration of the rim center
$\hat{\mathbf{a}}$	Relative acceleration
$\mathbf{a}_c$	Transport acceleration
$\boldsymbol{u}$	Elastic displacement
θ^w	Euler angle
ψ	Camber angle
φ	Slip angle
θ	Rotating angle
$\mathbf{w}$	Velocity caused by rigid body rotation
$u_{i,j}$, $u_{i,jk}$	Elastic displacement gradient
$\boldsymbol{\Omega}$	Rotation speed
x	Longitudinal rectangular position coordinates
$_y$	Transverse rectangular position coordinates
N_x, N_y	In-plane normal forces in the x and y directions (force/length)
N_{xy}	In-plane shear force relative to the x, y axes (force/length)
M_x, M_y	Bending moments in the x and y directions (moment/length)
M_{xy}	Twisting moment related to the x, y axes (moment/length)
ε_x^0, ε_y^0	Midplane normal strains in the x and y directions
γ_{xy}^0	Midplane shear strain relative to the x, y axes
k_x, k_y	Bending curvatures (1/length)
k_{xy}	Twisting curvature (1/length)
A_{11}, A_{22}, A_{12}, A_{21}	In-plane stretching stiffness (force/length)
A_{16}, A_{26}, A_{61}, A_{62}	In-plane bending stiffness (force/length)
A_{66}	In-plane shearing stiffness (force/length)
B_{11}, B_{22}, B_{12}, B_{21}	Bending-stretching coupling stiffnesses (force)
B_{16}, B_{26}, B_{62}, B_{62}	Bending-shearing coupling stiffness (force)
B_{66}	Twisting-shearing coupling stiffness (force)
D_{11}, D_{22}, D_{12}, D_{21}	Bending stiffness (force · length)
D_{16}, D_{26}, D_{61}, D_{62}	Bending-twisting coupling stiffness (force · length)
D_{66}	Twisting stiffness (force · length)
ϕ_z	Bending-twisting coupling angle
u_x, v_y	In-plane displacements in the x and y directions
$\bar{u}_1$	Lateral deformation of tire tread
$\bar{z}$	Position in longitudinal direction of contact region
$\mathbf{v}_T$	Transport velocity of tire tread moving through the contact area
$\mathbf{v}_1$	Lateral velocity of tire belt
F_1	Lateral force
c_1	Lateral stiffness of tire tread brush

Downloaded from http://meridian.allenpress.com/rct/article-pdf/94/1/180/2807318/0035-9475-94-1-180.pdf by Ministry of Science and Technology (Thailand) user on 25 May 2022